Biochemical and Biophysical Research Communications 464 (2015) 869–874

Contents lists available at ScienceDirect

Biochemical and Biophysical Research Communications

journal homepage: www.elsevier.com/locate/ybbrc

Crystal structure of β-N-acetylglucosaminidase CbsA from *Thermotoga neapolitana*

Jin-Sik Kim [a], Bo-Young Yoon [b], Jinsook Ahn [a], Jaeho Cha [c], Nam-Chul Ha [a, *]

[a] Department of Agricultural Biotechnology, Center for Food Safety and Toxicology, Center for Food and Bioconvergence, Research Institute for Agricultural and Life Sciences, Seoul National University, Seoul, Republic of Korea
[b] Institute of Fisheries Sciences, Pukyong National University, Busan, Republic of Korea
[c] Department of Microbiology, College of Natural Sciences, Pusan National University, Busan, Republic of Korea

ARTICLE INFO

Article history:
Received 26 June 2015
Accepted 9 July 2015
Available online 14 July 2015

Keywords:
cbsA
Thermotoga
Thermostable enzyme
β-N-Acetylglucosaminidase
Crystal structure

ABSTRACT

CbsA from the thermophilic marine bacteria *Thermotoga neapolitana* is a chitinolyitc enzyme that can cleave a glycosidic bond of the polymer N-acetylglucosamine at the non-reducing end. This enzyme has particularly high activity on di-N-acetylchitobiose. CbsA consists of a family of 3 glycoside hydrolase (GH3)-type catalytic domains and a unique C-terminal domain. The C-terminal domain distinguishes CbsA from other GH3-type enzymes. Sequence analyses have suggested that CbsA has the Asp–His dyad as a general acid/base with the NagZ of *Bacillus subtilis* and the *Salmonella enterica* serovar Typhimurium. Here, we determined the crystal structure of CbsA from *T. neapolitana* at a resolution of 2.0 Å using the Zn-SAD method, revealing a unique homodimeric assembly facilitated by the C-terminal domains in the dimer. We observed that CbsA is strongly inhibited by $ZnCl_2$, and two zinc ions were consistently bound in the active site. Our results can explain the zinc ion's inhibition mechanism in the subfamily of GH3 enzymes, and provide information on the structural diversity and substrate specificity of this hydrolase family.

1. Introduction

Chitin is a long chain polymer of N-acetylglucosamine (GlcNAc) and is massively produced in nature. For example, chitin is the main component of the cell walls of fungi and the exoskeletons of arthropods [1]. A wide range of organisms from bacteria to higher plants and animals produce chitinolytic enzymes for nutrition, morphogenesis, and defense against fungi [2]. In marine waters, over 10^{11} tons of chitin are estimated to be produced annually, mostly from copepods that are rapidly consumed [3].

The degradation process of chitin in Gram-negative bacteria is complex [4]. The extracellular chitinases mainly degrade into chitobiose ($GlcNAc_2$), which enters the periplasmic space across the outer membrane through chitoporins, and then is transported into the cytoplasm by an ABC transporter. In the cytoplasm, $GlcNAc_2$ is further degraded by chitinolyitc enzymes [5]. β-N-acetylglucosaminidases (EC. 3.2.1.52), belonging to the glycoside hydrolase family 3 (GH3), efficiently remove single GlcNAc residues from the non-reducing end of the chitin chain using a two-step, double replacement mechanism [5,6]. These enzymes are selective for GlcNAc with the signature sequence [KH(F/I)PG(H/L)G], which is expected to hold the N-acetyl group of the substrate [7,8]. Recently, the GH3-type β-N-acetylglucosaminidases CbsA and NagA were isolated in the thermophilic marine bacteria *Thermotoga neapolitana* and *Thermotoga maritima,* respectively. CbsA and NagA are highly active on $GlcNAc_2$ and chitotriose ($GlcNAc_3$) in the cytoplasm, and produce GlcNAc that can be metabolized via glycolysis [7].

A notable GH3 β-N-cetylglucosamindase is NagZs of *Bacillus subtilis* (BsNagZ), which has been well-characterized structurally [9]. BsNagZ is composed of the N-terminal $(\beta/\alpha)_8$ barrel fold (TIM-barrel, a typical catalytic domain of glycosidases) and the C-terminal αβα-sandwich fold. NagZ from *Salmonella enterica* serovar Typhimurium (StNagZ) lacks the C-terminal domain, belonging to the single-domain GH3 family [10]. These GH3 NagZ enzymes catalyze the removal of GlcNAc from a peptidoglycan fragment in Gram-negative bacteria [11], and has been implicated in the induction of AmpC-mediated β-lactamase [12,13]. The N-terminal TIM barrel domains have both nucleophilic residues and general

* Corresponding author. Building 200, Room 1041, 1 Gwanak-ro, Gwanak-gu, Seoul 151-921, Republic of Korea.
E-mail address: hanc210@snu.ac.kr (N.-C. Ha).

http://dx.doi.org/10.1016/j.bbrc.2015.07.053
0006-291X/

acid/base residues that are crucial for the catalytic process in GH3 enzymes, while the C-terminal domain does not seem to directly participate in the catalysis [10].

Sequence analyses have proposed that CbsA and NagA from *Thermotoga* share catalytic mechanisms as well as the overall structure with bacterial NagZs. However, it has previously been reported that CbsA forms a dimer in solution, which differs from the monomeric enzymes BsNagZ and StNagZ [7]. To investigate the molecular basis for the features observed in CbsA and NagA in comparison with other GH3-type enzymes, we determined the crystal structure of CbsA from *T. neapolitana*, which provides a deeper structural understanding of GH3-type enzymes.

2. Materials and methods

2.1. DNA construction, protein expression, and protein purification

The processes of DNA construction, protein expression, and protein purification have been described previously [14].

2.2. Crystallization, data collection, and structural determination

The crystallization of the native CbsA protein has been described previously [14]. Phases were determined using the anomalous signals from the bound Zn^{2+} in the crystals [15]. To derivatize crystals with Zn^{2+}, the crystals were soaked with 10 mM $ZnCl_2$ for 6 days. X-ray diffraction data from the crystals were collected on an ADSC Q-315 CCD detector installed in the beamline 5C of the Pohang Accelerator Laboratory (Republic of Korea). The 35 Zn^{2+} sites were found using the PHENIX program [16], which produces a high-quality electron density map. Four molecules were found in the asymmetric unit, which corresponded to a solvent content of 59%. The resulting model was built based on the catalytic domain of BsNagZ (PDB code: 3BMX) [9], which traced 60% of the structure. The remaining residues were manually built with the program COOT [17,18]. The R_{work} and R_{free} of the final model were 20.1% and 24.3%, respectively. The native CbsA structure was solved using the Zn-bound structure as a starting model. After rigid body refinement, positional and B-factor refinement was carried out using the PHENIX program [16]. Data collection and refinement statistics are summarized in Table 1.

2.3. β-N-acetylglucosaminidase assay

The protein sample was incubated with 10 mM EDTA for 60 min, and then dialyzed against 100 mM Hepes buffer (pH 7.5), 150 mM NaCl, and 2 mM β-mercaptoethanol. To measure the N-acetylglucosaminidase activity, the protein sample (50 μM) was incubated with 1 mM 4-Nitrophenyl N-acetyl-β-D-glucosaminide (pNP-GlcNAc), 100 mM HEPES pH 7.5, 1 mM $ZnCl_2$, or $MnCl_2$ at 70 °C over a period of 10 min at 415 nm for 1 min [19].

3. Results

3.1. Structural determination

We overproduced the full-length CbsA protein in *Escherichia coli*, and purified the protein by Ni^{2+}-affinity chromatography, followed by heat treatment and size exclusion chromatography. Crystals in the *R*32 space group were obtained at pH 7.5 in the presence of 0.1 M $CdCl_2$, and a native dataset was collected, as described previously [14]. The crystal structure was solved by the SAD method using the anomalous signals from the bound zinc ions in the Zn-soaked crystals. We were able to trace most of the residues into a high-quality electron density map, and refined the Zn-bound structure to a resolution of 2.5 Å. The structure of native CbsA protein was determined at 2.0 Å resolution using the Zn-bound structure. The asymmetric unit in the native crystal contained four protomers, which were nearly identical with a root-mean-square deviation (RMSD) ranging from 0.287 to 0.581 Å between the matched Cα atoms (Fig. 1A and B). Any significant structural variation was not found by superposition of the protomers in the asymmetric units (Fig. 1B). The final atomic model was comprised of residues 2–467 in the protomer, which were optimally ordered. Further details on the structural determination and refinement are given in Table 1.

Table 1
Data collection and structure refinement statistics.

Dataset	Native CbsA	Zn-soaked CbsA
Data collection		
X-ray source	BL44 at Spring-8	BL7A at PLS
Wavelength (Å)	0.9000	1.28248
Resolution (Å)	50–2.0 (2.03-2.00)	20–2.5 (2.54–5.50)
Space group	*R*32	*R*32
Cell parameter	$a = b = 158.5$, $c = 517.0$ Å, $\alpha = \beta = 90°$, and $\gamma = 120°$	$a = b = 158.8$, $c = 520.6$ Å, $\alpha = \beta = 90°$, and $\gamma = 120°$
Completeness (%)	93.6 (86.4)	99.8 (99.6)
R_{merge}[a] (%)	10.4 (34.0)	8.9 (30.9)
Redundancy	4.7 (2.6)	8.4 (6.2)
Average I/σ (I)	15.1 (2.2)	31.0 (5.0)
Refinement		
Resolution (Å)	20–2.0	20–2.5
R factor (%)	23.8	20.1
R_{free}[b] (%)	27.6	24.3
Average B factor (Å^2)	29.8	35.5
Wilson B factor (Å^2)	22.9	34.1
RMSD bonds (Å)	0.013	0.015
RMSD angles (°)	1.485	1.555
Ramachandran plot		
Most favored (%)	97.2	97.0
Allowed (%)	2.8	3.0
Coordinate error (Å)	0.28	0.27
PDB entry	5BZA	5C0Q

Values in parentheses refer to the highest resolution shell.
[a] $R_{merge} = \Sigma_{hkl} \Sigma_i |I_i(hkl) - < I(hkl)>| / \Sigma_{hkl} \Sigma_i I_i (hkl)$, where $I_i(hkl)$ and $<I(hkl)>$ are the observed intensity and the mean intensity of the related reflections, respectively.
[b] R_{free} was calculated with 5% of the data set.

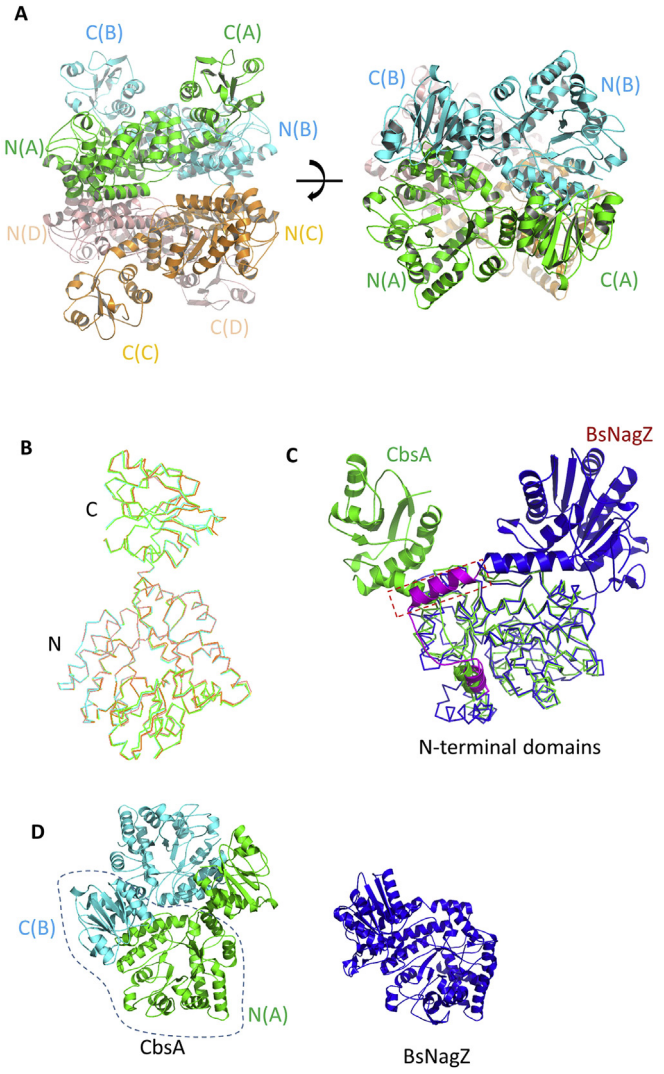

Fig. 1. Overall structure of CbsA. (A) Four protomers are included in the asymmetric unit of CbsA (*Left*, side view; *Right*, top view). Each protomer is in green (chain A), cyan (chain B), orange (chain C), or salmon (chain D). The N- and C-terminal domains are labeled N or C with the chain name in parentheses. (B) The superimposed Cα-trace representations of the four protomers in the asymmetric unit. (C) A CbsA protomer (green) is superimposed onto BsNagZ (blue) using the N-terminal domains (Cα-tracing) as a reference. The C-terminal domains are displayed in the ribbon representations, including the interdomain loop and α-helices. The interdomain loop and α-helices of BsNagZ are in magenta, and the dotted red box indicates the additional α-helix present in BsNagZ, as compared to CbsA. (D) A combination (a dotted line) of the N-terminal domain of one subunit and the C-terminal domain of the other subunit in the CbsA dimer (left) exhibit a structure similar to that of BsNagZ (right). (For interpretation of the references to colour in this figure legend, the reader is referred to the web version of this article.)

3.2. Overall structure of native CbsA and the structural comparison

The CbsA structure reveals two separate domains: the N-terminal domain and the C-terminal domain. The N-terminal domain (residues 2–325) carries the catalytic nucleophilic residue Asp245 in a $(\beta/\alpha)_8$-barrel fold known as a TIM-barrel, which is a common feature in many catalytic domains of glycosidases including GH3-type enzymes. Consistent with previous gel filtration results [7], the crystal structure of CbsA indicated that the enzyme forms a dimer. Extensive interactions between the two protomers in the crystal were observed (see below). In the asymmetric unit, the two dimers were packed vertically (Fig. 1A). The C-terminal domain in the one dimer was well-ordered, presumably due to parking interactions mediated by the C-terminal domains, while the C-terminal domain of the other dimer seemed to be mobile, as judged by the high values of the temperature factor.

The overall structure of the N-terminal domain as well as the amino acid sequence identity are very similar to the corresponding region of the two-domain BsNagZ (27% sequence identity, RMSD of 0.926 Å based on the Cα superimposition of 203 residues) and the single-domain StNagZ (23% sequence identity, RMSD of 1.634 Å based on the Cα superimposition of 173 residues). Although the amino acid sequence identity of the C-terminal domain was relatively low compared to that of BsNagZ (12%), the overall fold was well-conserved. When the overall structure of the CbsA protomer was compared with the other two-domain GH3 enzymes, the location of the C-terminal domain was found to be located on a different side of the N-terminal TIM barrel domains (Fig. 1C). A shorter α-helix between the N- and C-terminal domains of CbsA resulted in the relocation of the C-terminal domain, as compared to BsNagZ (Fig. 1C). However, a combination of the N-terminal domain of one subunit and the C-terminal domain of the other subunit in the dimeric assembly (see below) exhibited a similar domain arrangement to BsNagZ (Fig. 1D).

3.3. CbsA has a unique dimeric structure

A remarkable feature of CbsA is its unique dimeric assembly. The CbsA dimer is reminiscence of a saddle in an upside-down orientation (Fig. 2A). The two TIM barrels in the dimer are oriented side-by-side, forming a flat and elongated rectangle. Both the active sites of the CbsA dimer are on the tops of the TIM barrels, and are separated via a central groove in the N-terminal TIM barrel dimer. The C-terminal domains are located on both sides of the N-terminal TIM barrel dimer. As mentioned above, the combined structure of the N-terminal domain and the C-terminal domain from the other subunit in the dimer shows a similar domain arrangement with BsNagZ (Fig. 1D). Thus, the role of the C-terminal domain is expected to be similar to that of the bacterial two-domain GH3 in terms of catalytic activity, although the function of the C-terminal domain remains to be elucidated.

The dimerization interface of CbsA can be divided into two regions (Fig. 2B and C). The first interface is between the N-terminal domains of the dimer (Fig. 2B), involving both polar and hydrophobic interactions. Asn104 and Thr105 form a hydrogen bonding network with Arg101 of the other subunit. Arg101 forms another hydrogen bonding network with the Thr105 and Asn104 of the other subunit. Arg319 and Glu97 form an electrostatic interaction between the N-terminal domains. In addition, Lue102 and Leu106 form a hydrophobic interaction at the two-fold axis. The second dimerization interface is between the N-terminal domain and the C-terminal domain (Fig. 2C). Like the first dimerization interface, both polar and hydrophobic interactions are observed (Fig. 2C). Glu334, Arg431, and Lys451 in the C-terminal domain form polar interactions with Glu68, Glu70, Ser77, and Lys86 in the other subunit in the dimer. Ile325 and Val328 in the C-terminal domain form hydrophobic interactions with Pro76, Phe78, Pro79, and Phe91 of the other subunit (Fig. 2C). Further study is required to elucidate the biochemical function of the unique dimeric assembly of CbsA.

3.4. Active site with an Asp–His dyad as a general acid/base catalyst

CbsA has a loop with an Asp–His dyad that acts as a general acid/base catalyst in the N-terminal with the TIM-barrel domain-like BsNagZ and StNagZ [10]. The conformations of the Asp–His loop seems to depend on the presence of substrates in the active site. In a structural and modeling study of StNagZ, the unliganded

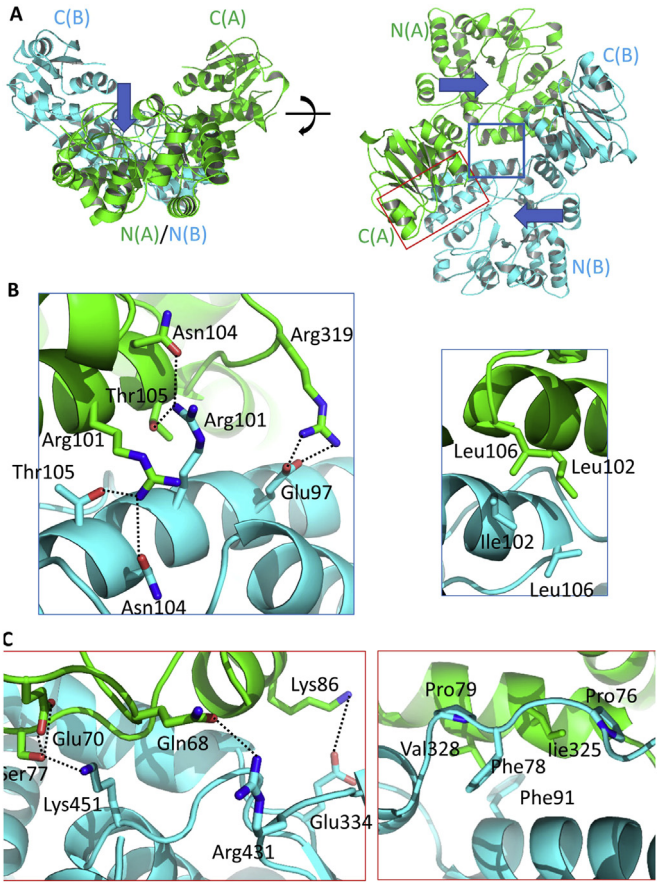

Fig. 2. The dimeric structure of CbsA. (A) Two perpendicular views of the CbsA dimer, which are presented in ribbons. Each protomer is colored in green and cyan. The active sites are indicated by the arrows. (B) The dimeric interface between the N-terminal domains in the dimer. The polar interactions are displayed in the left panel, and hydrophobic interactions are in the right panel. (C) The dimeric interface between the N-terminal domain and the C-terminal domain from the other subunit of the dimer. Polar interactions are shown in the left panel, while hydrophobic interactions are in the right panel. (For interpretation of the references to colour in this figure legend, the reader is referred to the web version of this article.)

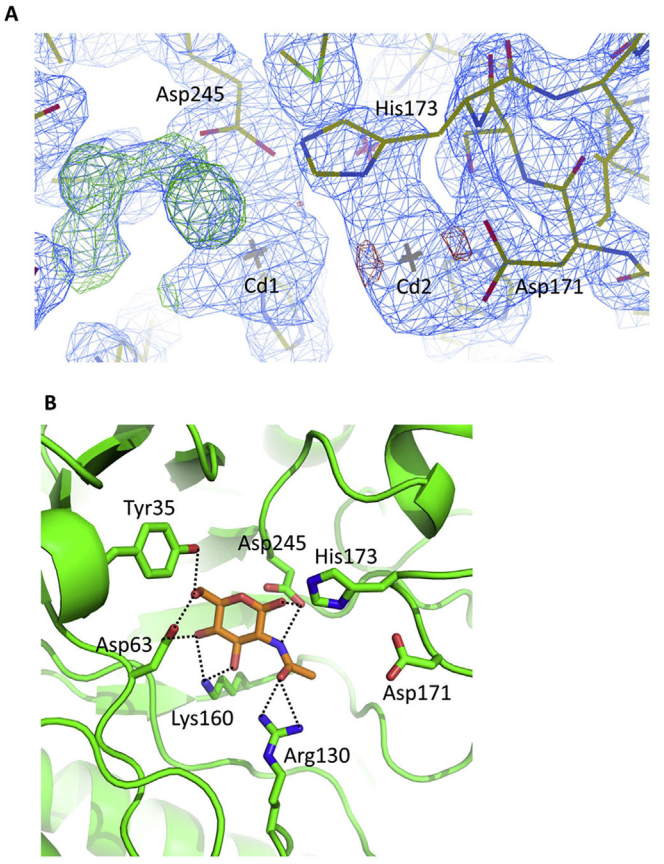

Fig. 3. The bound metals and the substrate. (A) The electron density maps at the active site cleft. Two bound Cd^{2+} or Zn^{2+} ions and the unidentified electron density are displayed. The 2*FoFc* map (blue) are contoured at 1.5 σ, and the *FoFc* maps are contoured at +4.0 σ (green) and −4.0 σ (red). (B) A modeled GlcNAc in the active site, whose positions were determined by superimposition with the GlcNAc-bound structure of StNagZ (PDB code 4GVF). The interactions with GlcNAc are shown in dotted lines. (For interpretation of the references to colour in this figure legend, the reader is referred to the web version of this article.)

structure of StNagZ was found to have a disordered catalytic loop, while the presence of substrate in the active site results in an extruded catalytic loop that repositions into the active site to create a distorted substrate conformation [10]. Interestingly, the crystal structure of CbsA exhibited a catalytic loop containing the Asp–His dyad in the liganded conformation, although external ligand was not added during purification and crystallization. This liganded conformation might have resulted from a bound metal ion (see below) and a blob visible in the electron density map in the active site of CbsA, which was not identifiable (Fig. 3A). These structural comparisons suggest that CbsA shares an active site structure and an enzymatic mechanism with BsNagZ and StNagZ, with the catalytic loop containing the Asp–His dyad functioning as a general acid/base catalyst.

By superimposing the GlcNAc-bound structure of StNagZ (PDB code: 4GVF), we modeled substrate (GlcNAc) binding in the CbsA structure (Fig. 3B). The GlcNac was nicely fitted into the active site pocket in the TIM barrel lined with Tyr35, Asp63, Arg130, Lys160, and Asp245. The Asp245 of CbsA corresponded to the catalytic nucleophilic residue aspartic acid (Asp318 of BsNagZ), while CbsA His173-Asp171 corresponded to the catalytic dyad (His234-Asp232 of BsNagZ).

3.5. Metal ion binding sites

The crystallization solution for CbsA contained 100 mM $CdCl_2$, and the crystals were immediately dissolved in a Cd-free solution. Consistently, we found 11 Cd^{2+} binding sites in the native structure of CbsA, as judged by the strong electron densities and chemical environments that are compatible with cadmium ions. One such site is in the crystal packing interface between the C-terminal domain from chain A and B in the crystal's neighboring molecule, which appears to be critical for crystal formation and the stabilization of the C-terminal domains of chain A and B (Suppl. Fig. S1).

To obtain phase information, the crystals were soaked with 10 mM $ZnCl_2$ in a 100 mM $CdCl_2$-containing crystallization solution. The strong anomalous signals at the Zn-absorption edge easily identified 11 zinc binding sites, revealing that 8 of 11 Cd^{2+} binding sites were replaced (Suppl. Fig. S2). These replacements by Zn^{2+}, despite the element's lower concentration, suggest that the binding affinities to Zn^{2+} are much stronger than those to Cd^{2+}. Two Zn^{2+} were found in the active site of CbsA. The first Zn^{2+} (Zn1) was surrounded by the carboxylate group of Asp171 and the imidazole ring of His173. The other Zn^{2+} (Zn2) was coordinated by the side chains of Asp245 and His161. Both Zn^{2+} ions could affect the chemical properties of the catalytic residues and prevent substrate binding (Fig. 4A). We next assessed the role of Zn^{2+} in the enzymatic activity of CbsA. The addition of 1 mM $ZnCl_2$ strongly inhibited CbsA activity, while $MnCl_2$ did not affect the activity of

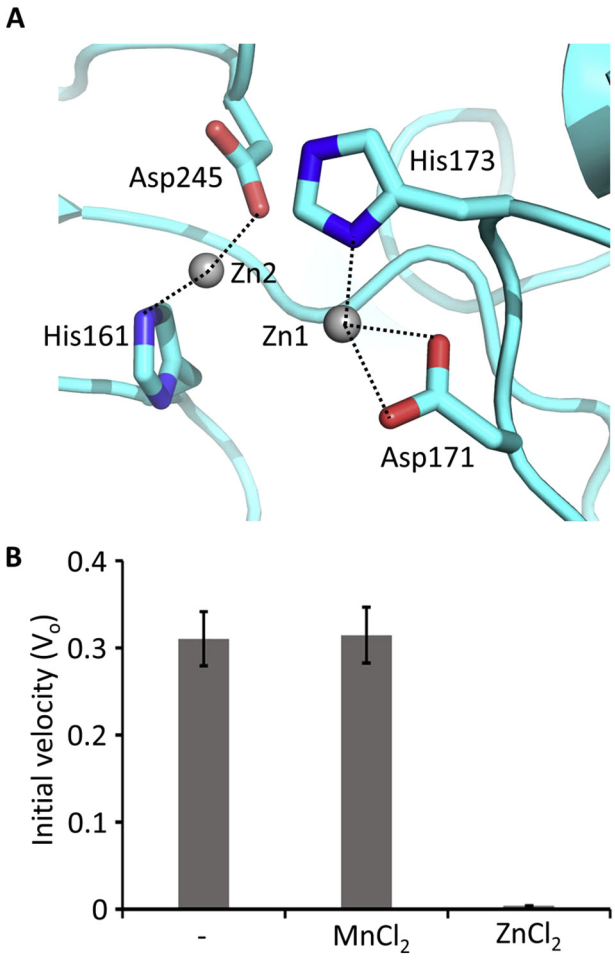

Fig. 4. Zinc binding sites and their inhibitory activity. (A) Two Zn^{2+} bound in the active site. One Zn^{2+} is bound by Asp245, the nucleophilic residue, and the other Zn^{2+} is surrounded by His175 and Asp171, which are general acid/base residues. (B) The chitolytic activity of CbsA in the presence of Zn^{2+} and Mn^{2+}. The purified CbsA protein was incubated with the chromogenic pNP-GlcNAc substrate in the absence (−) and presence of 1 mM $ZnCl_2$ or $MnCl_2$. The initial velocities were measured. The error bars represent the standard deviations from the three independent experiments.

CbsA. These results can be explained by Zn^{2+} binding in the Asp–His dyad (Fig. 4B). Given that the Asp–His dyad is conserved in StNagZ and BsNagZ, our result suggests that inhibition by Zn^{2+} could occur by the same mechanism.

4. Discussion

In this study, we determined the crystal structure of CbsA from *T. neapolitana*, which is a thermostable two-domain β-N-acetylglucosaminidase. The crystal structure provides information on the detailed structural features of CbsA, including its unique dimeric assembly. The location and orientation of the C-terminal domain are distinct from those of other two-domain GH3 enzymes. Nonetheless, the C-terminal domain of the other protomer in the dimer is in the similar position with a similar orientation as the monomeric BsNagZ, indicating that the C-terminal domain could be functionally involved. However, further studies may be required to elucidate the role of this domain. The structure also suggested that all of the residues involved in catalytic activity and substrate recognition are in the N-terminal domain with the catalytic loop containing the Asp–His dyad, similar to in StNagZ and BsNagZ. Many metal ion binding sites were identified in the structure, and biochemical study suggested that the molecular nature of Zn^{2+} inhibited the activity of the GH3 enzymes. The modeling study also suggested a putative substrate binding structure, which might be useful in investigating a detailed catalytic mechanism and substrate recognition.

Since the characterization of the crystal structure of the two-domain barley β-D-glucan glucohydrolase (HvExoI), many GH3 enzyme structures have been investigated [20]. The domains and substrate specificities in the structures of these GH3 members are diverse. HvExoI catalyzes the hydrolytic removal of non-reducing glucosyl end residues from a broad range of β-D-glucans and β-D-glucosides [21]. In the structure of HvExoI, a short helix in the C-terminal domain carries the general acid/base catalyst [22]. However, the corresponding helix of the C-terminal domain is absent in CbsA, but has a loop containing the catalytic Asp–His dyad in the N-terminal TIM-barrel domain, as observed in BsNagZ and StNagZ [10].

Our findings in this study will facilitate the development of selective inhibitors that target the NagZ of pathogenic bacteria, and will also contribute to the development of better enzymes for the industrial degradation of chitin, which is massively produced in nature, by CbsA. Furthermore, this study provides a structural basis for a detailed exploration of the substrate specificity and selectivity of these members of the hydrolase family for different natural carbohydrate polymers.

Acknowledgements

This study was supported by the Ministry of Science, ITC, and Future Planning, Republic of Korea (NRF-2014R1A2A1A11050283), and by the SNU Invitation Program for Distinguished Scholars. This study utilized beamline 5C at PLS (Pohang, Korea) and BL44 at Spring-8 (Osaka, Japan).

Appendix A. Supplementary data

Supplementary data related to this article can be found at http://dx.doi.org/10.1016/j.bbrc.2015.07.053.

Transparency document

Transparency document related to this article can be found online at http://dx.doi.org/10.1016/j.bbrc.2015.07.053.

References

[1] S.A. Shaikh, M.V. Deshpande, Chitinolytic enzymes – their contribution to basic and applied-research, World J. Microb. Biot. 9 (1993) 468–475.
[2] S. Adrangi, M.A. Faramarzi, A.R. Shahverdi, Z. Sepehrizadeh, Purification and characterization of two extracellular endochitinases from Massilia timonae, Carbohyd Res. 345 (2010) 402–407.
[3] X.B. Li, S. Roseman, The chitinolytic cascade in Vibrios is regulated by chitin oligosaccharides and a two-component chitin catabolic sensor/kinase, Proc. Natl. Acad. Sci. U. S. A. 101 (2004) 627–631.
[4] S. Beier, S. Bertilsson, Bacterial chitin degradation-mechanisms and ecophysiological strategies, Front. Microbiol. 4 (2013) 149.
[5] S. Adrangi, M.A. Faramarzi, From bacteria to human: A journey into the world of chitinases, Biotechnol. Adv. 31 (2013) 1786–1795.
[6] D.J. Vocadlo, S.G. Withers, Identification of active site residues in glycosidases by use of tandem mass spectrometry, Methods Mol. Biol. 146 (2000) 203–222.
[7] K.H. Choi, J.Y. Seo, K.M. Park, C.S. Park, J. Cha, Characterization of glycosyl hydrolase family 3 beta-N-acetylglucosaminidases from Thermotoga maritima and Thermotoga neapolitana, J. Biosci. Bioeng. 108 (2009) 455–459.
[8] S. Belkin, C.O. Wirsen, H.W. Jannasch, A new sulfur-reducing, extremely thermophilic eubacterium from a submarine thermal vent, Appl. Environ. Microbiol. 51 (1986) 1180–1185.
[9] S. Litzinger, S. Fischer, P. Polzer, K. Diederichs, W. Welte, C. Mayer, Structural and kinetic analysis of bacillus subtilis N-acetylglucosaminidase reveals a unique Asp-His dyad mechanism, J. Biol. Chem. 285 (2010) 35675–35684.

[10] J.P. Bacik, G.E. Whitworth, K.A. Stubbs, D.J. Vocadlo, B.L. Mark, Active site plasticity within the glycoside hydrolase NagZ underlies a dynamic mechanism of substrate distortion, Chem. Biol. 19 (2012) 1471–1482.
[11] Q.M. Cheng, H.S. Li, K. Merdek, J.T. Park, Molecular characterization of the beta-N-acetylglucosaminidase of *Escherichia coli* and its role in cell wall recycling, J. Bacteriol. 182 (2000) 4836–4840.
[12] A. Asgarali, K.A. Stubbs, A. Oliver, D.J. Vocadlo, B.L. Mark, Inactivation of the glycoside hydrolase NagZ attenuates antipseudomonal beta-lactam resistance in *Pseudomonas aeruginosa*, Antimicrob. Agents Chemother. 53 (2009) 2274–2282.
[13] K.A. Stubbs, M. Balcewich, B.L. Mark, D.J. Vocadlo, Small molecule inhibitors of a glycoside hydrolase attenuate inducible AmpC-mediated beta-lactam resistance, J. Biol. Chem. 282 (2007) 21382–21391.
[14] B.Y. Yoon, L. Jiao, H.R. Moon, J. Cha, N.C. Ha, Crystallization and preliminary X-ray crystallographic analysis of the ss-N-acetylglucosaminidase CbsA from Thermotoga neapolitana, Acta Crystallogr. F. 68 (2012) 56–58.
[15] S.S. Cha, Y.J. An, C.S. Jeong, M.K. Kim, S.G. Lee, K.H. Lee, B.H. Oh, Experimental phasing using zinc anomalous scattering, Acta Crystallogr. D. 68 (2012) 1253–1258.
[16] P.D. Adams, R.W. Grosse-Kunstleve, L.W. Hung, T.R. Ioerger, A.J. McCoy, N.W. Moriarty, R.J. Read, J.C. Sacchettini, N.K. Sauter, T.C. Terwilliger, PHENIX: building new software for automated crystallographic structure determination, Acta Crystallogr. D. Biol. Crystallogr. 58 (2002) 1948–1954.
[17] J.E. Debreczeni, P. Emsley, Handling ligands with coot, Acta Crystallogr. D. Biol. Crystallogr. 68 (2012) 425–430.
[18] P. Emsley, K. Cowtan, Coot: model-building tools for molecular graphics, Acta Crystallogr. D. Biol. Crystallogr. 60 (2004) 2126–2132.
[19] Y.L. Jin, Y.Y. Jo, K.Y. Kim, J.H. Shim, Y.W. Kim, R.D. Park, Purification and characterization of beta-N-acetylhexosaminidase from rice seeds, J. Biochem. Mol. Biol. 35 (2002) 313–319.
[20] M. Hrmova, R. De Gori, B.J. Smith, A. Vasella, J.N. Varghese, G.B. Fincher, Three-dimensional structure of the barley beta-D-glucan glucohydrolase in complex with a transition state mimic, J. Biol. Chem. 279 (2004) 4970–4980.
[21] M. Hrmova, V.A. Streltsov, B.J. Smith, A. Vasella, J.N. Varghese, G.B. Fincher, Structural rationale for low-nanomolar binding of transition state mimics to a family GH3 β-d-glucan glucohydrolase from barley†,‡, Biochemistry 44 (2005) 16529–16539.
[22] J.N. Varghese, M. Hrmova, G.B. Fincher, Three-dimensional structure of a barley beta-D-glucan exohydrolase, a family 3 glycosyl hydrolase, Struct. Fold. Des. 7 (1999) 179–190.